EUROPEAN ORGANIZATION FOR NUCLEAR RESEARCH

CERN/EP 89-108
24th August 1989

A STUDY OF THE CENTRALLY PRODUCED $K^{*o}\bar{K}^{*o}$ FINAL STATE IN THE REACTION $pp \to p_f(K^+K^-\pi^+\pi^-)p_s$ AT 300 GeV/c

WA76 Collaboration

T.A. Armstrong[4,(*)], M. Benayoun[5], W. Beusch[4], I.J. Bloodworth[3], J.N. Carney[3], R. Childs[3], B.R. French[4], B. Ghidini[2], A. Jacholkowski[4], J. Kahane[5], J.B. Kinson[3], A. Kirk[3], K. Knudson[4], V. Lenti[2], Ph. Leruste[5], A. Malamant[5], J.L. Narjoux[5], F. Navach[2], A. Palano[2], E. Quercigh[4], N. Redaelli[4(**)], L. Rossi[4(***)], M. Sené[5], R. Sené[5], M. Stassinaki[1], M.T. Trainor[4], G. Vassiliadis[1], O. Villalobos Baillie[3], M.F. Votruba[3], G. Zito[2] and R. Zitoun[6]

1 Athens University, Physics Department, Athens, Greece

2 Dip. di Fisica dell'Università and Sezione INFN, Bari, Italy

3 University of Birmingham, Physics Department, Birmingham, UK

4 CERN, European Organization for Nuclear Research, Geneva, Switzerland

5 Collège de France, Paris, France

6 LPNHE, Universités de Paris VI et VII, Paris, France

ABSTRACT

The reaction $pp \to p_f(K^+K^-\pi^+\pi^-)p_s$, where the $K^+K^-\pi^+\pi^-$ system is centrally produced, has been studied at 300 GeV/c. The $K^{*o}\bar{K}^{*o}$ final state has been observed and the cross sections for its central production are found to be the same at 300 and 85 GeV/c. The $K^{*o}\bar{K}^{*o}$ final state appears to be produced as a non-resonant threshold enhancement.

Submitted to Zeitschrift für Physik C

(*) Present address: Pennsylvania State Univ., University Park, USA.
(**) Present address: INFN and Dip. di Fisica, Milan, Italy.
(***) Present address: INFN and Dip. di Fisica, Genova, Italy.

4302P/BRF/ed

1. INTRODUCTION

Production of pairs of vector meson resonances has been intensively studied in J/ψ decays and hadronic and two-photon reactions, by several experimental groups. One of the strongest motivations behind these studies is a search for gluonic and 4-quark states. For a recent review see ref. [1], in which a brief survey of theoretical models is also given.

Experiment WA76 has been designed to study exclusive final states formed in the reaction

$$pp \rightarrow p_f(X^o)p_s,$$

where the subscripts f and s indicate the fastest and slowest positive particles in the laboratory, and X^o represents the central system which is assumed to be produced by double exchange processes. At high centre-of-mass energies these double exchange processes are believed to be dominated by Double Pomeron Exchange, where the Pomeron is thought to have a large gluonic component, leading to the conclusion that Pomeron-Pomeron scattering could be a rich source for the production of gluonic states.

In this paper we present the results of the analysis of the $K^+K^-\pi^+\pi^-$ final state at 300 GeV/c, show evidence for associated vector-vector meson production and compare these results with the results previously published at 85 GeV/c [2].

2. DATA SELECTION

The data come from the WA76 Experiment which has been performed using the CERN Omega Spectrometer. Details of the trigger conditions and the data processing have been given in a previous publication [3]. The trigger was designed to enhance double exchange processes with respect to single exchange and elastic processes.

The exclusive reaction

$$pp \rightarrow p_f(K^+K^-\pi^+\pi^-)p_s \qquad (1)$$

has been isolated from the sample of events with six outgoing tracks in the final state. The slow proton, which triggered a system of scintillation counters, was identified by means of a pulse-height momentum correlation; the fast particle was assumed to be of the same nature as the incident beam.

Momentum balancing events were selected requiring |missing p_x| < 20.0 GeV/c, |missing p_y| < 0.16 GeV/c and |missing p_z| < 0.06 GeV/c, where the x axis is along the beam direction. After these cuts the sample consisted of 83 072 events. In order to overcome mass identification ambiguities, the following procedure was adopted:

(a) Using available Cherenkov information, an event was accepted if it contained at least one (positive or negative) particle identified as K or ambiguous K/p among the four particles.

(b) In each event, the four centrally produced tracks were momentum ordered. Using the method of Ehrlich et al. [4] with cuts on Ehrlich mass squared,

$$0.16 < M^2 < 0.56 \ (GeV/c^2)^2, \qquad (2)$$

we extracted 2184 events with one fast K^+ and one fast K^-. From the remaining events we extracted 1514 events with one fast $K^{\pm}$ and one slow $K^{\mp}$, and then 94 events with one slow K^+ and one slow K^-. In these configurations, the other two remaining central tracks were required, if reaching the Cherenkov system, to have a mass assignment compatible with the pion. Fig. 1 shows the total distribution of Ehrlich mass squared, where the first peak centred at the square of the pion mass is due to a residual contamination from the $2\pi^+2\pi^-$ channel and the two other stuctures are due to the signals of the reactions having centrally produced $K^+K^-\pi^+\pi^-$ and $p\bar{p}\pi^+\pi^-$ systems, respectively.

This selection procedure gave in total 3792 events belonging to reaction (1). The estimated contamination from the 4π channel is 12%. The distribution of the Feynman x, for the slow proton, the central system and the fast particle, is shown in fig. 2, where the central system is produced mainly in the range $|x_F| \leq 0.2$.

3. MASS SPECTRA

The 2-body effective mass spectra are shown in fig. 3. Resonance production is observed mainly in the two-body mass distributions, e.g. $K^{*o}(892)$ in the $K\pi$ combinations, and $\Delta^{++}(1232)$ and $\Delta^{o}(1232)$ in the mass spectra which include the fast track (not shown). There is some indication of $\phi(1020)$ and $\rho^{o}(770)$ production in the $K^{+}K^{-}$ and $\pi^{+}\pi^{-}$ combinations respectively, and no resonance production is observed in the 3-body combinations. Fig. 4 shows the 4-body effective mass distribution.

The scatter diagram of $M(\pi^{+}\pi^{-})$ vs $M(K^{+}K^{-})$ (not shown) reveals no accumulation of events in the region corresponding to associated production of $\phi(1020)$ and $\rho^{o}(770)$ final states. On the other hand, figs 5 and 6, which are the scatter diagram and the Lego plot respectively of $M(K^{-}\pi^{+})$ vs $M(K^{+}\pi^{-})$, show an accumulation of events in the $K^{*o}\bar{K}^{*o}$ region. Fig. 7 shows the $K\pi$ effective mass distribution for which the other $K\pi$ combination lies in the $K^{*o}(892)$ band; the selection used is

$$0.83 < M(K\pi) < 0.95 \text{ GeV/c}^2. \qquad (3)$$

A strong $K^{*o}(892)$ signal is seen with a relatively low background, which confirms the presence of a strong $K^{*o}\bar{K}^{*o}$ signal. The method of "nine regions" [2] was used to determine the amount of $K^{*o}\bar{K}^{*o}$ production. Table 1 shows the event distribution on the $K^{-}\pi^{+}$ vs $K^{+}\pi^{-}$ scatter plot of fig. 5, in 9 bins centred around the $K^{*o}(892)$ mass. Taking into account the effects due to $K^{*o}(892)$ Breit-Wigner tails, the total number of $K^{*o}\bar{K}^{*o}$ events above background was found to be 305 ± 46. The $K^{*o}\bar{K}^{*o}$ mass spectrum for the central mass region in Table 1 (481 events) is shown in fig. 8(a) and shows that the $K^{*o}\bar{K}^{*o}$ events are concentrated into a relatively narrow enhancement near threshold.

4. CHANNEL LIKELIHOOD FIT

In order to separate the different channels which contribute to reaction (1) and to make a quantitative analysis, we have used the technique of the Channel Likelihood Fit [5] using a modified version of the program CHAFIT [6].

The program performs a maximum likelihood fit of different overlapping amplitudes. We have used Breit-Wigner amplitudes with parameters fixed to standard PDG [7] values to describe the resonances observed. Each of the amplitudes has to be normalized by integration over the Lorentz invariant phase space. Because our reaction channels are restricted by the trigger conditions to a rather limited region of phase space it is difficult, using standard Monte Carlo techniques, to reproduce the phase space distribution in all the mass combinations. Therefore, a Monte Carlo generator was used, in which artificial events were generated where each of the six outgoing tracks was randomly taken from different real events. The events resulting from this generator where then used as phase space to integrate the input amplitudes for the fit. The results of the fit for reaction (1) are summarized in Table 2.

As seen from Table 2, we find no evidence for associated $\phi\,\rho^{o}$ production, but there is evidence for associated $K^{*o}\bar{K}^{*o}$ production at a level of (8.1 ± 0.9)%, corresponding to 308 ± 34 events. This is in agreement with the number of $K^{*o}\bar{K}^{*o}$ events above background, obtained in the previous section.

5. COMPARISON WITH THE 85 GeV/c DATA

To facilitate a comparison with the present data, the proton beam sample of the 85 GeV/c data [2] was re-analyzed using the procedure outlined in sect. 2.

Momentum balancing events were obtained requiring $|\text{missing } P_x| <$ 3.0 GeV/c, $|\text{missing } P_y| < 0.10$ GeV/c and $|\text{missing } P_z| < 0.08$ GeV/c. After these cuts the 85 GeV/c proton beam sample contained 43547 events. The above mentioned selection procedure gave in total 3187 events for the $K^+K^-\pi^+\pi^-$ channel, for reaction (1). The estimated contamination from the 4π channel is 13%. Using the cut (3) gave 370 events in the $K^{*o}\bar{K}^{*o}$ region and their mass spectrum is shown in fig. 8(b). The subtraction method of "nine regions" (Table 3) gave 149 ± 22 $K^{*o}\bar{K}^{*o}$ events above background, after taking into account the effects due to $K^{*o}(892)$ Breit-Wigner distribution tails. Comparing figs 8(a) and 8(b) it is seen that the 300 GeV/c and

85 GeV/c mass spectra of the $K^{*o}\bar{K}^{*o}$ final state are similar, both showing the same threshold enhancement. Fig. 9 shows a sum of the 300 and 85 GeV/c data in 25 MeV/c^2 bins.

The continuous curve superimposed in fig. 8(a) shows the result of the Monte Carlo generation of the $K^+K^-\pi^+\pi^-$ system using event mixing with $K^{*o}(892)$ selection cuts. It can be seen that the Monte Carlo generated spectrum gives the same threshold enhancement, which would seem to indicate that although we see clear $K^{*o}\bar{K}^{*o}$ production, we have no evidence for resonance production in the $K^{*o}\bar{K}^{*o}$ final state. Thus, the $K^{*o}\bar{K}^{*o}$ final state appears to be mainly produced as a non-resonant threshold enhancement in this experiment.

We have studied, in both the 85 and 300 GeV/c data samples, the angular distribution of $K^{*o}(892)$ in the $K^{*o}\bar{K}^{*o}$ rest system, using the helicity frame. We define θ_H as the polar angle between the K^{*o} direction in the $K^{*o}\bar{K}^{*o}$ rest frame relative to the $K^{*o}\bar{K}^{*o}$ momentum in the overall centre-of-mass system. The resulting $\cos\theta_H$ distributions of the K^{*o} (not shown) are flat, compatible with an S-wave decay of the $K^{*o}\bar{K}^{*o}$ final state.

6. THE CROSS SECTIONS AND COMPARISON WITH OTHER EXCLUSIVE FINAL STATES

In order to calculate the cross sections, a cut of $0.0 \leq x_F \leq 0.2$ has been placed on the Feynman x of the central system to select a region for which the acceptance is good for both the 85 and 300 GeV/c experiments. After correcting for the geometrical acceptance of the apparatus, processing and detector efficiencies, 4C cuts, Ehrlich mass cuts, low t losses, Breit-Wigner tails and unseen decay modes, the resulting $K^{*o}\bar{K}^{*o}$ cross sections are

$$\begin{aligned} &85 \text{ GeV/c:} \quad \sigma(K^{*o}\bar{K}^{*o}) = 33.4 \pm 8.0 \text{ nb}, \quad \text{and} \\ &300 \text{ GeV/c:} \quad \sigma(K^{*o}\bar{K}^{*o}) = 34.3 \pm 8.0 \text{ nb} . \end{aligned} \tag{4}$$

The cross sections for $K^{*o}\bar{K}^{*o}$ production at these two beam momenta are the same within errors, which is consistent with the $K^{*o}\bar{K}^{*o}$ final state being produced by a Double Pomeron exchange mechanism. The same conclusion was found to be valid for the centrally produced $\phi\phi$ system [8].

In Table 4 we summarize the cross sections for various centrally produced vector-vector meson final states [8,9], in the interval $0.0 \leq x \leq 0.2$, derived for the spectra above the $\phi\phi$ mass threshold, for the 300 GeV/c data. The ratios of cross sections are

$$\rho^o\rho^o/K^{*o}\bar{K}^{*o}/\phi\phi = 4 : 1 : 1 \ . \qquad (5)$$

7. CONCLUSIONS

We have observed production of the $K^{*o}\bar{K}^{*o}$ final state produced centrally in the hadronic reaction $pp \to p_f(K^+K^-\pi^+\pi^-)p_s$ at 300 GeV/c. The cross sections for $K^{*o}\bar{K}^{*o}$ production at 85 and 300 GeV/c (both in the region $0.0 \leq x_F \leq 0.2$) are the same within errors. The $K^{*o}\bar{K}^{*o}$ mass spectrum shows an accumulation of events near threshold. This final state appears to be mainly produced as a non-resonant threshold enhancement, and decays isotropically in its own rest system into two $K^{*o}(892)$ resonances. The cross section for formation of the $K^{*o}\bar{K}^{*o}$ final state above the $\phi\phi$ mass threshold is the same as the cross section for the centrally produced $\phi\phi$ final state.

REFERENCES

[1] W.H. Toki, Invited Talk, BNL Glueball Review, Proc. of the 1988 BNL Workshop on Glueballs, Hybrids and Exotic Hadrons; AIP Conf. Proc. No. 185, New York 1989, p. 692 (and SLAC-PUB-4824 preprint, December 1988);

R.S. Longacre, paper prsented at the 1988 BNL GLueball Workshop, Proc. of the 1988 BNL Workshop, p. 670 (and BNL 42241 preprint, December 1988;

B.A. Li and K.F. Liu, Phys. Rev. D28 (1983) 1636; Phys. Lett. 118B (1982) 435, Phys. Rev. Lett. 51 (1983) 1510;

N.N. Achasov et al., Zeitschr. für Phys. C27 (1985) 99.

[2] T.A. Armstrong et al., Zeitschr. für Phys. C34 (1987) 33.

[3] T.A. Armstrong et al., Nucl. Instr. and Meth. A274 (1989) 165.

[4] R. Ehrlich et al., Phys. Rev. Lett. 20 (1968) 686.

[5] P.E. Condon and P. Cowell, Phys. Rev. D9 (1974) 2258.

[6] Ph. Gavillet and J.C. Marin, CHAFIT, CERN/D.Ph.II/PROG 75-2 (1975).

[7] Review of Particle Properties, Phys. Lett. B204 (1988).

[8] T.A. Armstrong et al., Phys. Lett. B221 (1989) 221.

[9] T.A. Armstrong et al., Evidence for new states produced in the central region in the reaction pp → $p_f(\pi^+\pi^-\pi^+\pi^-)p_s$ at 300 GeV/c, CERN/EP 89-81, July 1989, to be published in Phys. Letters B.

TABLE CAPTIONS

TABLE 1 Event distribution on the $K^-\pi^+$ vs $K^+\pi^-$ scatter plot centred around the $K^{*o}(892)$ mass (300 GeV/c data).

TABLE 2 Results from the channel likelihood fit (300 GeV/c data).

TABLE 3 Event distribution on the $K^-\pi^+$ vs $K^+\pi^-$ scatter plot centred around the $K^{*o}(892)$ mass (85 GeV/c data).

TABLE 4 Cross sections for centrally produced vector-vector final states at 300 GeV/c ($0.0 \leq x_F \leq 0.2$).

TABLE 1

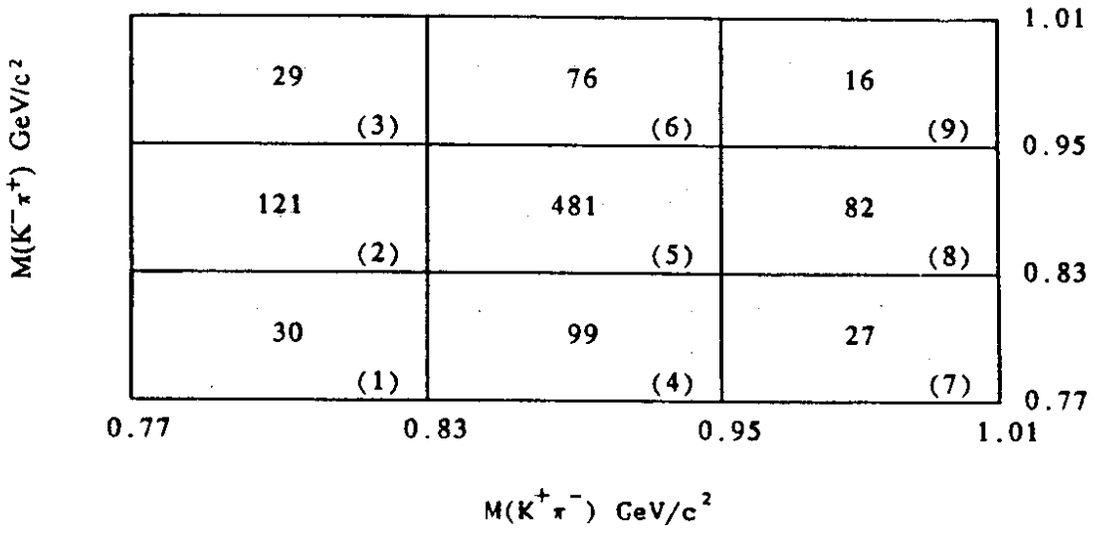

TABLE 2

Channel/final state	%
$K^{*o}K^-\pi^+p_fp_s$	11.9 ± 1.2
$\bar{K}^{*o}K^+\pi^-p_fp_s$	11.9 ± 1.2
$\rho^o\ K^+K^-p_fp_s$	7.9 ± 1.2
$\phi\pi^+\pi^-p_fp_s$	0.3 ± 0.4
$\Delta^{++}K^+K^-\pi^-p_s$	1.4 ± 0.4
$K^{*o}\bar{K}^{*o}p_fp_s$	8.1 ± 0.9
$\phi\rho^op_fp_s$	0.0 ± 0.2
Phase space	58.5 ± 2.1

TABLE 3

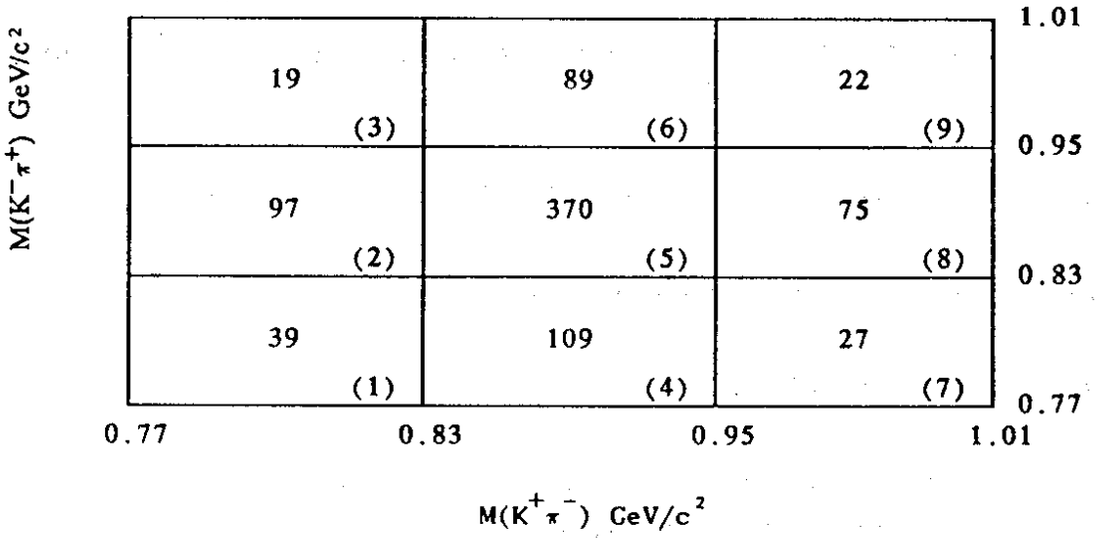

TABLE 4

Central final state	Cross section above the M(φφ) threshold
$K^{*o}\bar{K}^{*o}$	18 ± 6 nb
φφ	18 ± 6 nb
$\rho^o\rho^o$	78 ± 30 nb

FIGURE CAPTIONS

Fig. 1 The Ehrlich mass squared distribution.

Fig. 2 The Feynman x distribution for p_s, the $K^+K^-\pi^+\pi^-$ system and p_f.

Fig. 3 The two-body effective mass distributions: (a) $K^+\pi^-$; (b) $K^-\pi^+$; (c) $\pi^+\pi^-$; (d) K^+K^-.

Fig. 4 The four-body $K^+K^-\pi^+\pi^-$ effective mass distribution.

Fig. 5 The scatter diagram $M(K^-\pi^+)$ vs $M(K^+\pi^-)$.

Fig. 6 The Lego plot $M(K^-\pi^+)$ vs $M(K^+\pi^-)$.

Fig. 7 The $K\pi$ effective mass distribution when the other $K\pi$ combination lies in the $K^{*o}(892)$ band.

Fig. 8 The $K^{*o}\bar{K}^{*o}$ effective mass distributions: (a) 300 GeV/c data and (b) 85 GeV/c data. The superimposed curve in (a) is the normalized Monte Carlo $K^{*o}\bar{K}^{*o}$ effective mass distribution (see text).

Fig. 9 The sum of the $K^{*o}\bar{K}^{*o}$ effective mass distributions at 300 and 85 GeV/c.

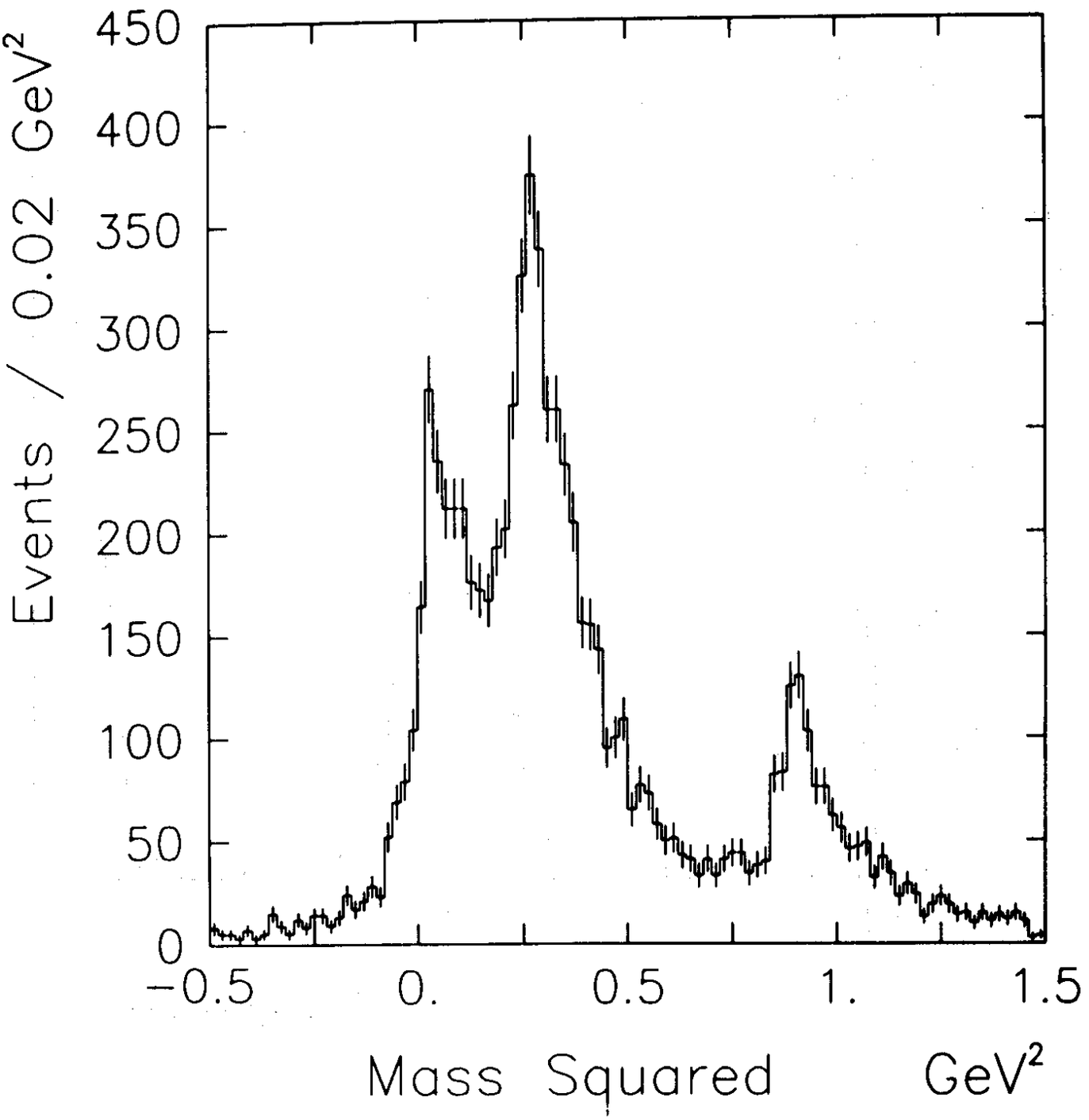
Events / 0.02 GeV²
450
400
350
300
250
200
150
100
50
0
−0.5
0.
0.5
1.
1.5
Mass Squared
GeV²

Fig. 1

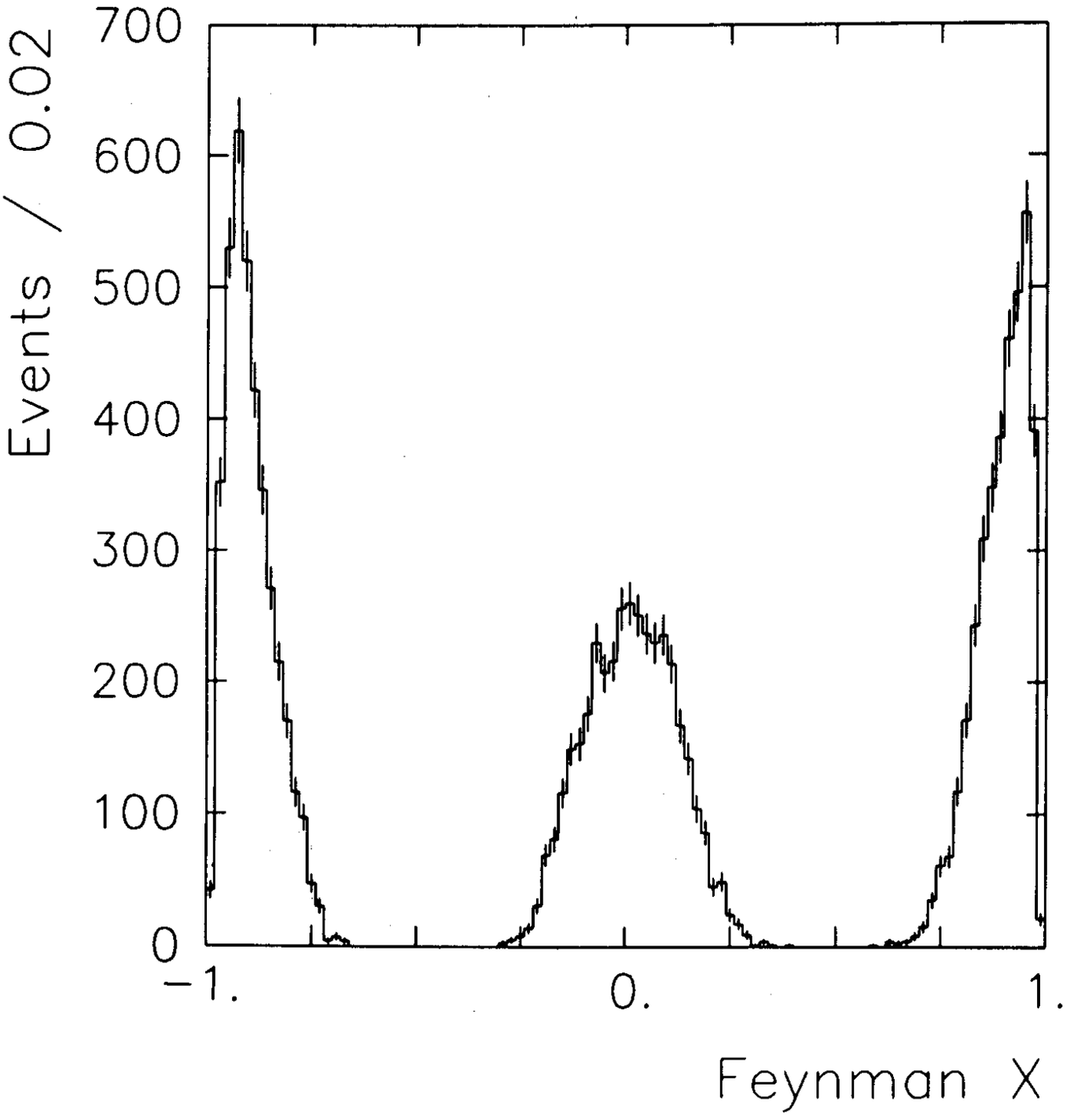

Fig. 2

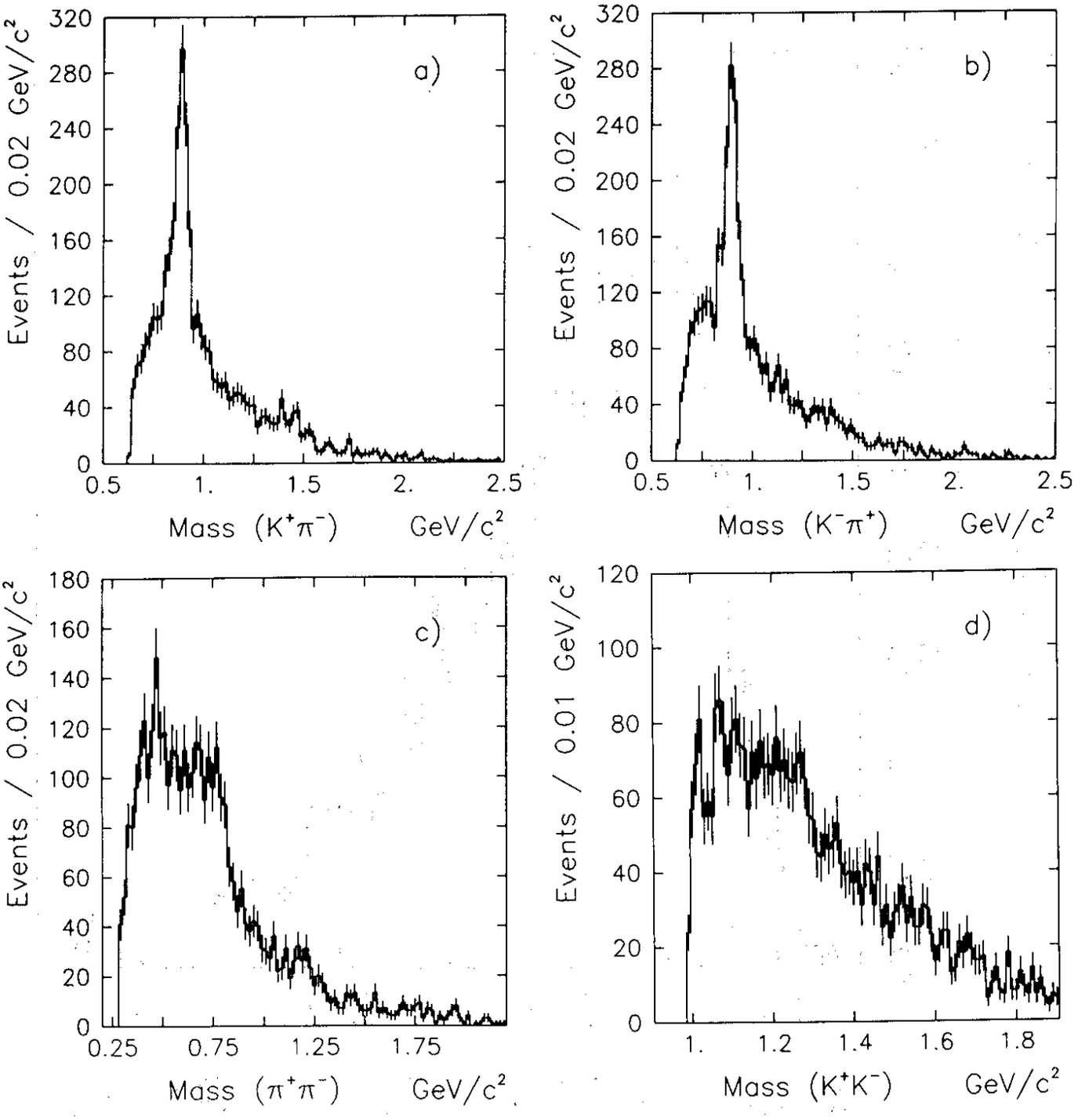
a)
b)
c)
d)
Events / 0.02 GeV/c²
Events / 0.01 GeV/c²
Mass (K⁺π⁻) GeV/c²
Mass (K⁻π⁺) GeV/c²
Mass (π⁺π⁻) GeV/c²
Mass (K⁺K⁻) GeV/c²

Fig. 3

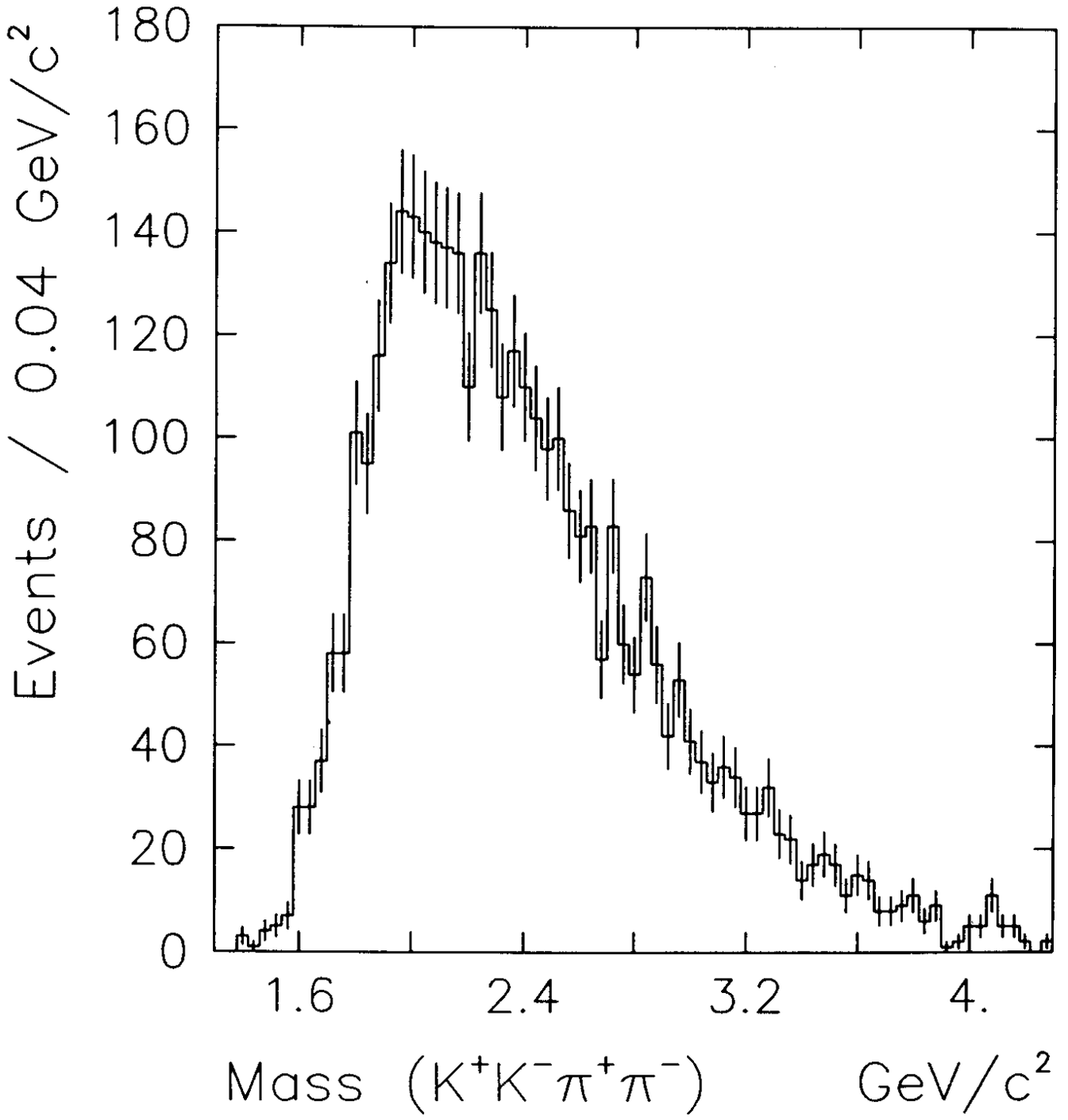
Events / 0.04 GeV/c²
180
160
140
120
100
80
60
40
20
0
1.6
2.4
3.2
4.
Mass (K⁺K⁻π⁺π⁻) GeV/c²

Fig. 4

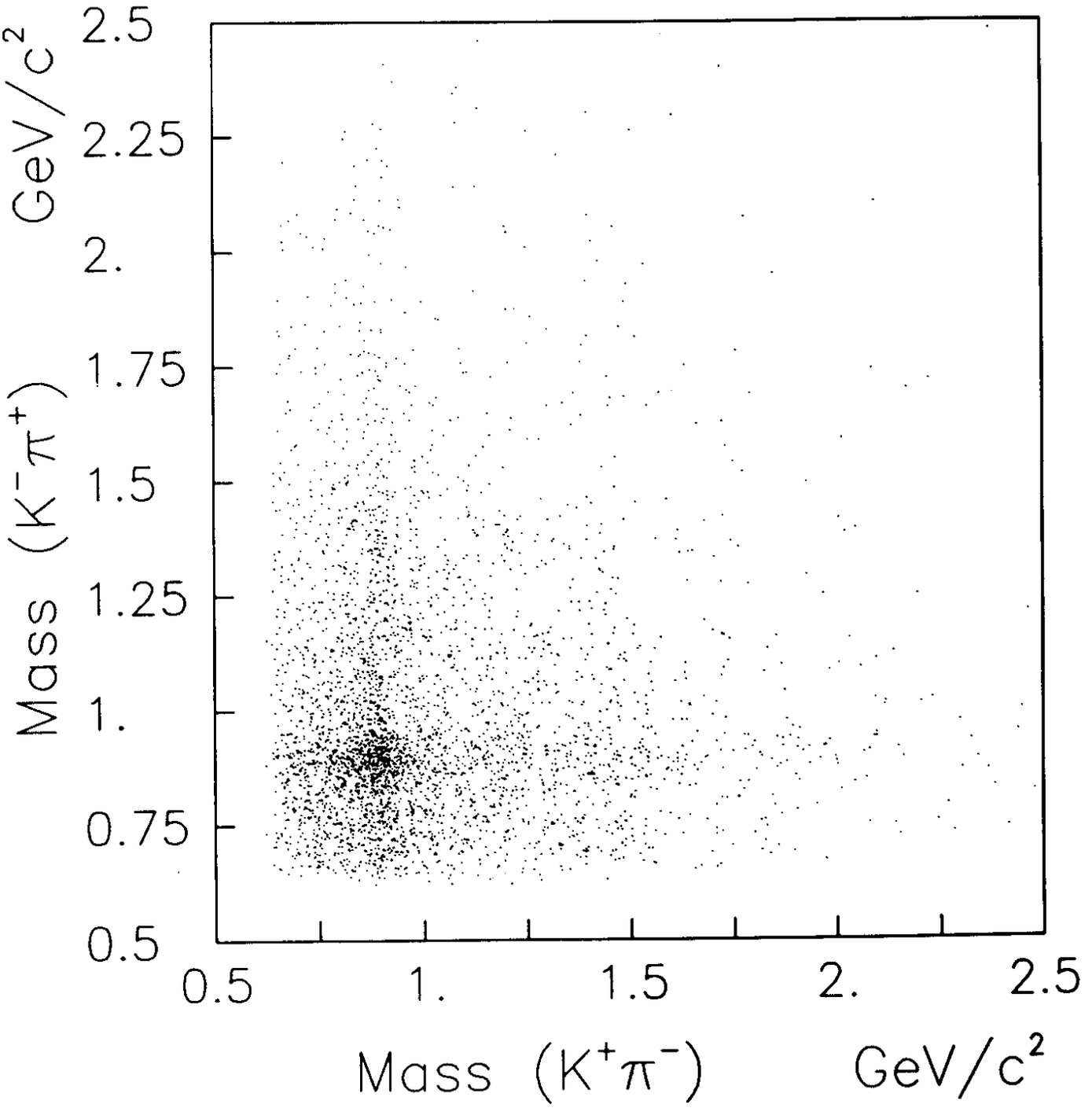
2.5
2.25
2.
1.75
1.5
1.25
1.
0.75
0.5
GeV/c²
Mass (K⁻π⁺)
0.5
1.
1.5
2.
2.5
Mass (K⁺π⁻)
GeV/c²

Fig. 5

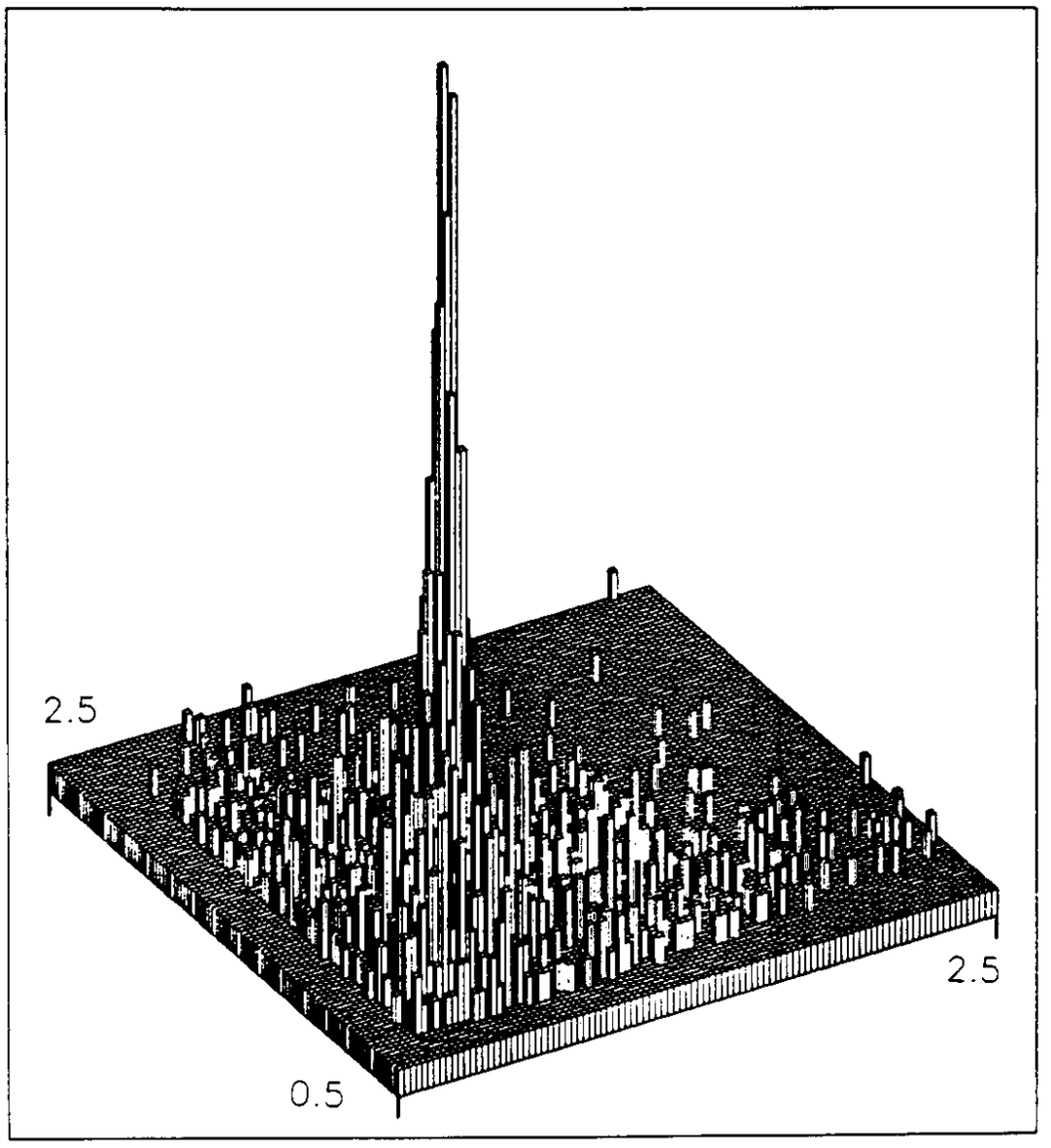

Fig. 6

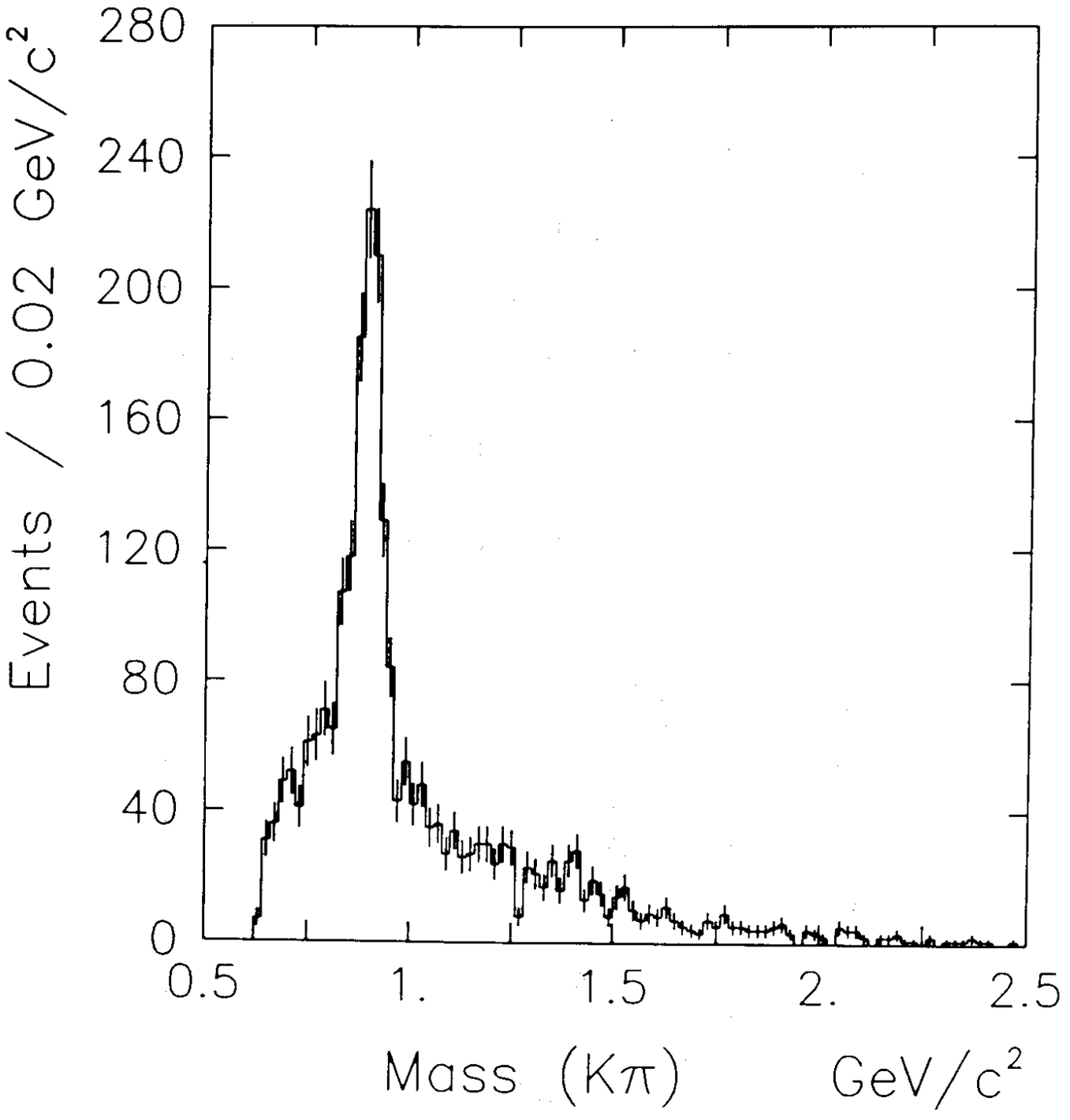
Events / 0.02 GeV/c²
280
240
200
160
120
80
40
0
0.5
1.
1.5
2.
2.5
Mass (Kπ) GeV/c²

Fig. 7

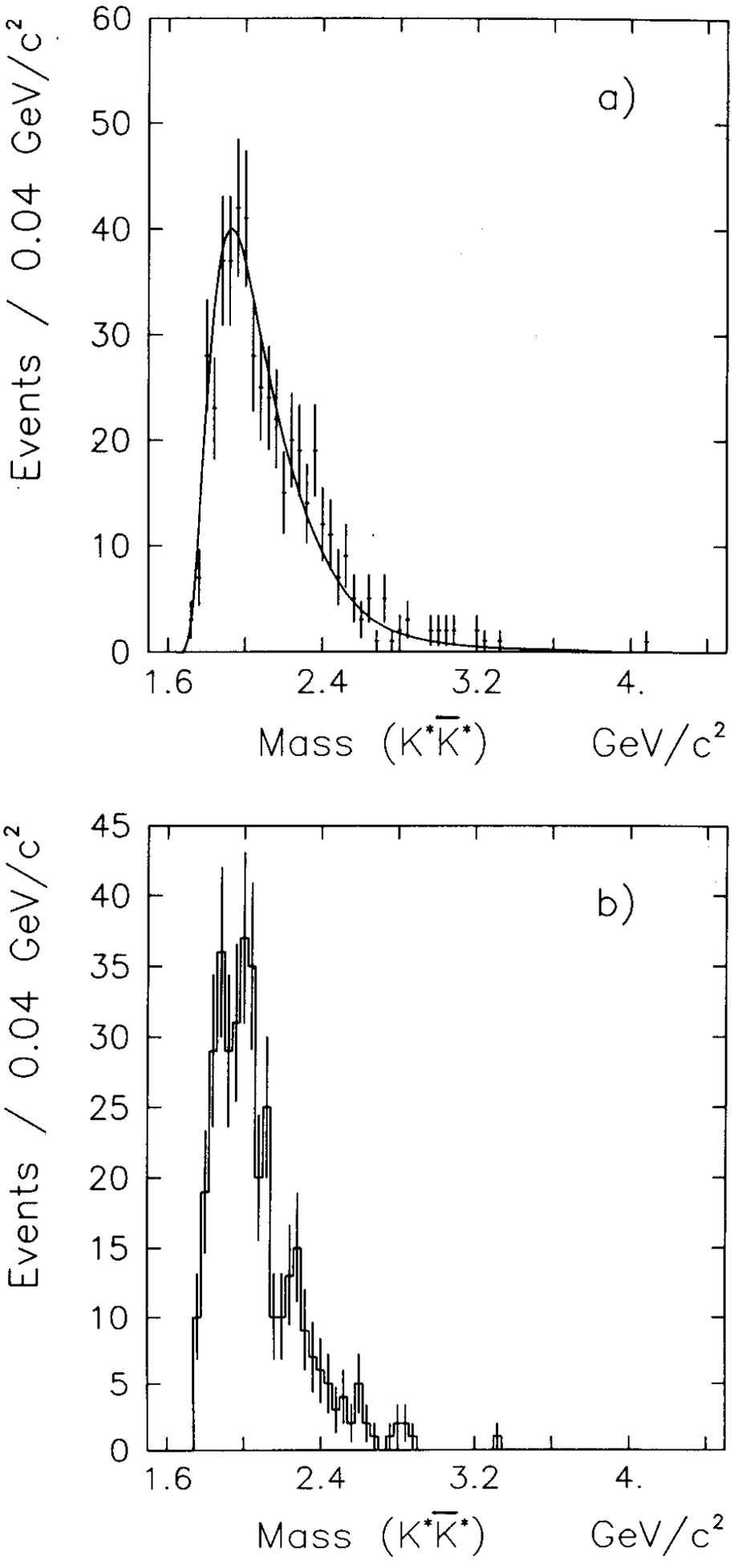
a)
Events / 0.04 GeV/c²
60
50
40
30
20
10
0
1.6
2.4
3.2
4.
Mass (K*K̄*) GeV/c²
b)
Events / 0.04 GeV/c²
45
40
35
30
25
20
15
10
5
0
1.6
2.4
3.2
4.
Mass (K*K̄*) GeV/c²

Fig. 8

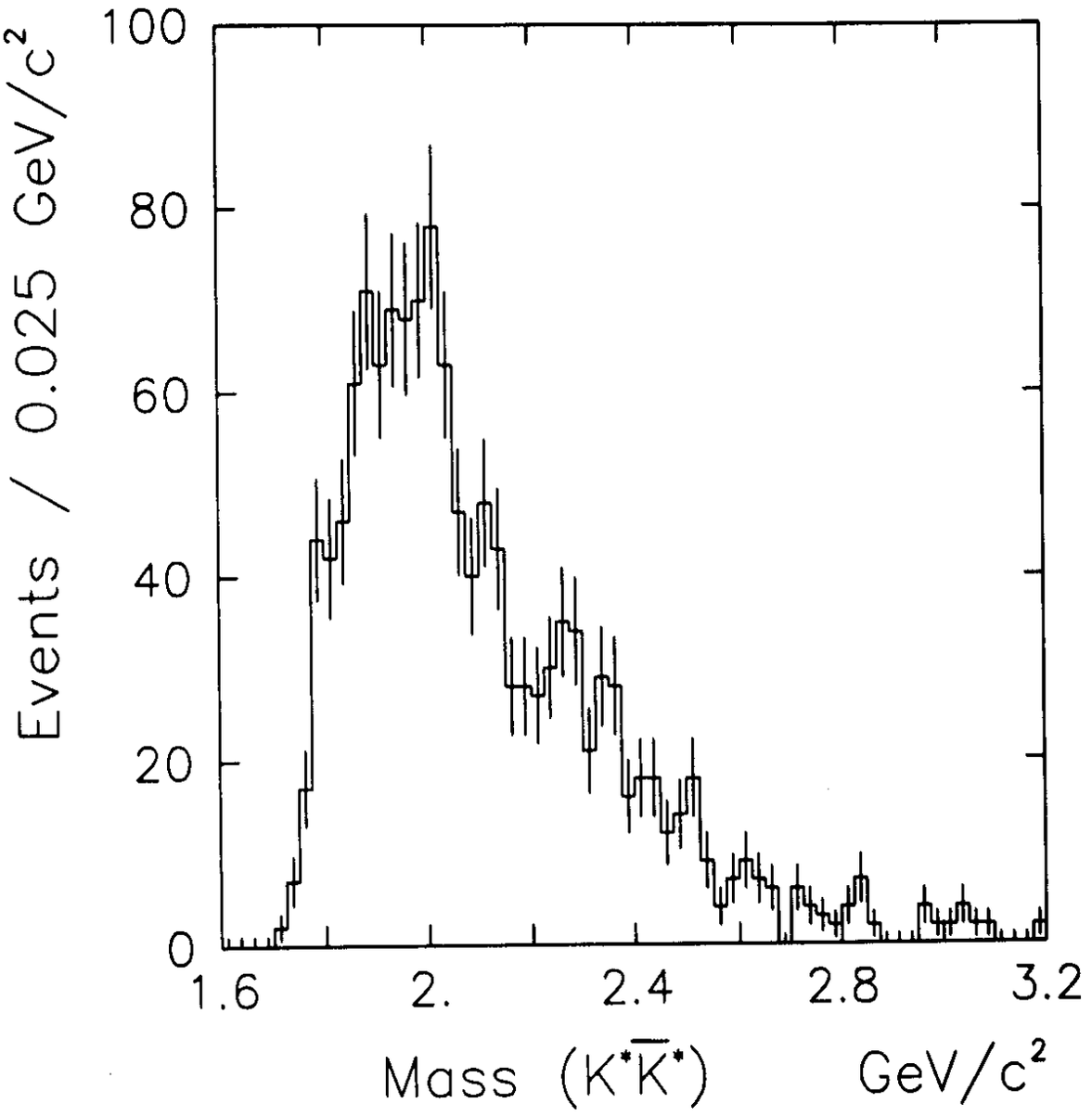

Fig. 9